Cytomegalovirus Restricts the Innate Immune Response by Nuclear Export of Host Restriction Factor DDX41

Vargab Baruah[1] and Christine M. O'Connor[1,2,3]*

[1] Infection Biology; Sheikha Fatima bint Mubarak Global Center for Pathogen and Human Health Research, Lerner Research Institute, Cleveland Clinic, Cleveland, OH, 44195 USA; baruahv@ccf.org (V.B.); oconnoc6@ccf.org (C.M.O'C.)
[2] Case Comprehensive Cancer Center, Cleveland, OH 44106 USA; oconnoc6@ccf.org (C.M.O'C.)
[3] Molecular Medicine, Cleveland Clinic Lerner College of Medicine of Case Western Reserve University, Cleveland Clinic, Cleveland, OH 44195 USA; oconnoc6@ccf.org (C.M.O'C.)
* Corresponding author: oconnoc6@ccf.org

Abstract

The innate immune response is the first line of defense against invading pathogens, including the betaherpesvirus, human cytomegalovirus (CMV). The host's innate response acts as the first line of defense, and CMV, like other viruses, has consequently evolved multiple mechanisms to manipulate host interferon (IFN) responses. DEAD-box Helicase 41 (DDX41) is an intracellular dsDNA sensor that, upon activation by Bruton's tyrosine kinase (BTK), triggers type I IFN production through the Stimulator of Interferon Genes (STING) signaling pathway. Here, we show the activation of this signaling pathway during lytic CMV infection, wherein BTK, DDX41, and STING are activated through tyrosine phosphorylation, and both DDX41 and BTK interact with STING. Further, CMV infection re-localizes DDX41 from the nucleus to the cytoplasm, where it localizes to the perinuclear virus assembly compartment (vAC). Here, DDX41 phosphorylation is attenuated, suggesting cytoplasmic redistribution leads to a less active or inactive form. Additionally, DDX41 co-localizes in the vAC with the CMV tegument proteins, pp65 and pp71, each of which interact with DDX41 in immunoprecipitation assays. We further demonstrate the protective role of this signaling pathway, as treatment with the BTK inhibitor, orelabrutinib, attenuates DDX41 phosphorylation/activation and supports increased expression of viral proteins and virus replication. In sum, our work highlights the important role of BTK-DDX41-STING signaling in the innate immune response against CMV, which the virus subverts by attenuating its cytoplasmic activity, thereby diverting it from its typically protective function.

Importance

Human cytomegalovirus (CMV) is a ubiquitous pathogen that poses a significant threat to immunocompromised individuals, highlighting the critical role of innate immunity in controlling this viral infection. Despite extensive research, the complex mechanisms underlying innate immunity against CMV and the virus's strategies for evading immune detection remain only partially understood. This study identifies the activation of the cellular BTK-DDX41-STING innate signaling axis during lytic CMV

infection, which ultimately results in protective interferon responses. Our findings show that CMV infection triggers the cytoplasmic redistribution of the cellular protein, DDX41, leading to reduced phosphorylation and activity, thereby undermining its protective function. Additionally, pharmacological inhibition of BTK enhances viral protein expression and replication, highlighting the importance of this pathway in immune defense. Our work identifies BTK- and DDX41-dependent STING signaling as important for innate immune responses against CMV and further advances our understanding of CMV's manipulation of these responses.

Keywords

CMV, DDX41, STING, BTK, cytomegalovirus

50 **Introduction**

51 Human cytomegalovirus (CMV), a widespread beta-herpesvirus, infects 40% to 60% of adults in
52 developed countries, with seropositivity nearing 100% in developing nations (1). Following primary CMV
53 infection, the virus enters a latent phase within myeloid cells, characterized by viral genome
54 maintenance and suppressed infectious virus production. Latent CMV can intermittently reactivate
55 under certain conditions of immune system dysfunction and cellular differentiation, resulting in the lytic
56 replication of infectious virus (2). While primary infection and reactivation events are typically
57 asymptomatic, they can be severe in immunocompromised, immunosuppressed, or immuno-naïve
58 individuals, potentially causing serious organ-specific diseases or even death. A substantial proportion
59 of the population, even in developed countries, is immunologically vulnerable. In the US, about 3% of
60 adults are immunocompromised, and 6.6% are immunosuppressed due to health conditions or their
61 treatments (3, 4). Among immuno-naïve neonates, approximately 1 in 200 babies has congenital CMV
62 infection (5), and up to 15% of these infants develop long-term sequelae (6). These data underscore
63 the need to more completely understand the viral and cellular factors that support CMV replication.

64 The severity and outcome of CMV infection largely depend on the early immune events, when
65 the host's innate immunity plays a crucial role (7). It can prevent the establishment of infection by
66 overwhelming CMV upon initial contact or confine the virus to the latent phase, preventing progression
67 to the lytic phase. Early immune responses often involve recognition of pathogen-associated molecular
68 patterns (PAMPs) – conserved molecular signatures found on pathogens - by the host's pattern
69 recognition receptors (PRRs), which heavily influence the subsequent immune strategy. CMV's double-
70 stranded DNA (dsDNA) genome is detected by dsDNA-sensing PRRs, triggering an immune signaling
71 cascade that results in the production of anti-viral interferons (IFNs) and interferon-stimulated genes
72 (ISGs) (8). Understanding these key immune responses at the molecular level is crucial, particularly in
73 the absence of a vaccine, to determine how CMV might subvert these mechanisms as it infects the
74 host.

75 Activation of key components of the innate immune response is intricately linked to the CMV life
76 cycle, with different viral components targeted based on their abundance and accessibility. CMV dsDNA
77 can bind cytosolic DNA receptors such as cyclic GMP-AMP synthase (cGAS) and interferon-γ inducible
78 protein 16 (IFI16). This DNA sensing is followed by activation of stimulator of interferon genes (STING;
79 also known as MITA and ERIS), a key mediator in subsequent downstream immune signaling. STING
80 activation leads to the recruitment and activation of TANK-binding kinase 1 (TBK1), which in turn
81 phosphorylates interferon regulatory factor 3 (IRF3). This activated IRF3 then translocates to the
82 nucleus, where it drives the expression of type I interferons (IFN) and other inflammatory cytokines,
83 thereby mounting a defense against the invading virus (9).

84 Host-driven immune responses against CMV are complex since CMV has evolved impressively
85 sophisticated methods of manipulating host factors. For instance, CMV's tegument protein pp65 and
86 late protein pUL31 bind cGAS, inhibiting its activity (10, 11). Additionally, the membrane protein pUL42
87 also binds cGAS, blocking both its DNA binding and its ability to oligomerize/activate (12). Similar
88 observations are reported for IFI16, where pp65 binds IFI16 and inhibits its DNA sensing by preventing
89 its aggregation and signal amplification (13, 14). CMV also modulates restriction factors downstream of
90 DNA sensing. The viral glycoprotein, US9, the tegument protein, pp71, and the latency-associated
91 protein, pUL138, each bind STING and impair immune signaling (15-17). In addition to directly inhibiting
92 immune signaling through binding, CMV also subverts the immune response by misdirecting the
93 localization of restriction factors. For instance, while nuclear IFI16 binds CMV DNA early in infection,
94 during later stages, it is phosphorylated by pUL97 and mis-localized to the cytoplasmic vAC (18). While
95 these studies highlight the intricate and diverse mechanisms the host employs against CMV, as well as
96 those the virus uses to counter them, our understanding of the array of innate immune sensors triggered
97 by CMV is likely incomplete.

98 DEAD-box helicase 41 (DDX41) is a helicase with a conserved Asp-Glu-Ala-Asp (DEAD) motif
99 that functions as a DNA sensor (19). Similar to other DNA sensors such as cGAS and IFI16, DDX41
100 activity is regulated by tyrosine phosphorylation. Lee at al. have demonstrated that Bruton's tyrosine
101 kinase (BTK) phosphorylates DDX41 enhancing its binding to adenovirus dsDNA and STING (20).
102 Additionally, herpes simplex virus type 1 (HSV-1) infection results in upregulation of DDX41, upon which
103 it interacts with cGAS, activates the STING signaling pathway, and promotes inflammatory cytokine
104 production (19). However, the role of the BTK-DDX41-STING signaling axis in CMV infection remains
105 unknown. Given that DDX41 shares many downstream effectors with cGAS and IFI16, and that CMV
106 has a dsDNA genome, we posited that this signaling pathway could function as part of the innate
107 immune response against CMV.

108 Here, we show that the BTK-DDX41-STING signaling axis is activated during lytic CMV
109 infection, involving tyrosine phosphorylation of the restriction factors, and interaction of STING with
110 DDX41 and BTK. Infection re-localizes DDX41 from the nucleus to the cytoplasm, where it co-localizes
111 with the tegument protein, pp65, in the perinuclear vAC. Additionally, cytoplasmic-localized DDX41
112 displays reduced phosphorylation, indicating that its CMV-induced redistribution leads to a less active
113 form of the protein. Finally, we demonstrate that inhibiting BTK with orelabrutinib reduces
114 phosphorylation and activation of BTK and DDX41, which increases viral protein expression and
115 replication. Our work reveals an important role of the BTK-DDX41-STING pathway in the innate immune
116 response to CMV and demonstrates a mechanism by which the virus disrupts this response.
117

118 **Materials and Methods**

119 *Cells and Viruses*

120 Primary newborn human foreskin fibroblasts (NuFF-1, passage 13-28; GlobalStem, Rockville, MD,
121 USA) were cultured in Dulbecco's modified Eagle medium (DMEM) with 10% fetal bovine serum (FBS),
122 2 mM L-glutamine, 0.1 mM non-essential amino acids, 10 mM HEPES, and 100 U/ml each of penicillin
123 and streptomycin. The cells were maintained at 37°C with 5% CO_2.

124 The bacterial artificial chromosome (BAC)-derived viruses, TB40/E*mCherry* (WT) (21) and
125 TB40/E*mCherry*-UL99eGFP (UL99*gfp*) (22, 23) were previously characterized. Virus stocks were
126 prepared as previously described (24). In brief, p0 stocks were generated by transfecting BAC DNA into
127 naïve NuFF-1 cells. When 100% cytopathic effect (CPE) was observed, p1 stocks were expanded on
128 naïve NuFF-1 cells and harvested when 100% CPE was observed. Virus was purified through a 20%
129 sorbitol (VWR) cushion, resuspended 1:1 in XVIVO-15 (Lonza) and 3% bovine serum albumin (BSA),
130 aliquoted, flash frozen in liquid nitrogen, and stored at -80°C. Virus stocks were titered on naïve NuFF-
131 1 cells by 50% tissue culture infectious dose ($TCID_{50}$) assay.

132 Cells were infected at the multiplicity of infection (MOI) and for the duration indicated in the text.
133 Cells were infected in DMEM containing viral inoculum for 1 h at 37°C, with gentle agitation every 15
134 minutes (min). The cells were washed twice with 1X phosphate-buffered saline (PBS) and replenished
135 with fresh DMEM at 37°C.

136 *Protein and RNA Analyses*

137 For protein analyses, cells were harvested at the times indicated in the text and/or Figure Legends and
138 were lysed on ice for 1 hour (h) using radioimmunoprecipitation assay (RIPA) buffer (1.0% NP-40; 1.0%
139 sodium deoxycholate; 0.1% SDS; 0.15 M NaCl; 0.01 M NaPO4, pH 7.2; 2 mM EDTA), with vortexing
140 every 15 min. For protein isolation in nuclear/cytoplasmic fractions, cell pellets were resuspended in
141 lysis buffer (10 mM HEPES, pH 7.5; 5 mM MgCl2; 15 mM KCl; 1 mM PMSF) and subjected to three
142 freeze-thaw cycles in liquid nitrogen. The resulting suspension was passed through a 27G needle 15
143 times. The lysed cells were layered over 50% sucrose (w/v) and centrifuged; the supernatant collected
144 as the cytoplasmic fraction. The pellet containing nuclei was resuspended in lysis buffer and sonicated
145 three times. After centrifugation, the supernatant was collected as the nuclear fraction. In all cases,
146 protein concentrations were measured by Bradford assay with Protein Assay Dye Reagent Concentrate
147 (Bio-Rad). Samples were denatured at 95°C for 10 min. Equal protein concentrations of the samples
148 were separated by SDS-PAGE and transferred to 0.45 µm nitrocellulose membranes (Amersham) using
149 a semi-dry transfer method. The following antibodies were used at the specified concentrations: anti-

150 BTK (Cell Signaling Technology [CST], 1:5,000), anti-STING (CST, 1:5,000; MilliporeSigma, 1:5,000),
151 anti-DDX41 (CST, 1:5,000), anti-TBK (CST, 1:5,000), anti-CMV IE1 (clone 1B12, 1:100, (25)), anti-CMV
152 UL44 (Virusys, 1:2500), anti-CMV pp65 (clone 8A8, 1:50 (26)), anti-CMV pp71, anti-tubulin
153 (MilliporeSigma, 1:5000), anti-H3 (Abcam, 1:5000), anti-beta-actin-peroxidase (MilliporeSigma,
154 1:10,000), goat-anti-mouse horseradish peroxidase (HRP) secondary and goat-anti-rabbit horseradish
155 peroxidase (HRP) secondary (both from Jackson ImmunoResearch Labs, 1:10,000). Relative protein
156 levels were quantified by densitometry using ImageJ (27).

157 To quantify transcripts, total RNA was isolated and purified using the High Pure RNA Isolation kit
158 (Roche) in accordance to the manufacturer's protocol. Equal RNA concentrations (1.0 µg) were then
159 used to generate cDNA with random hexamer primers and SYBR™ Green I Reagents (ThermoFisher
160 Scientific), and equal volumes of cDNA were used for quantitative polymerase chain reaction (qPCR).
161 The following primers were used for transcript quantification: *IFNB*, forward – 5'-
162 CTTGGATTCCTACAAAGAAGCAGC-3' and reverse – 5'- TCCTCCTTCTGGAACTGCTGCA -3';
163 *UL123*, forward – 5'-GCCTTCCCTAAGACCACCAAT-3' and reverse – 5'-
164 ATTTTCTGGGCATAAGCCATAATC-3'; *GAPDH*, forward – 5'-CTGTTGCTGTAGCCAAATTCGT-3'
165 and reverse – 5'-ACCCACTCCTCCACCTTTGAC-3'. Samples were analyzed in triplicate using a 96-
166 well-format CFX Connect Real Time PCR machine (Bio-Rad), and expresion quantified relative to host
167 *GAPDH* expression.

168 *Immunofluorescence Assays*

169 Cells were cultured on coverslips in 6-well tissue culture plates (3×10^5 cells per well) and infected (MOI
170 = 0.5 $TCID_{50}$/cell) as described above. After 96 hpi, cells were washed three times with 1X PBS, fixed
171 with 2% paraformaldehyde for 15 min at 37°C, and then permeabilized with 0.1% Triton X-100 for 15
172 min at room temperature. The cells were washed three times with 0.25% (w/v) saponin and
173 subsequently blocked with 1X PBS containing 10% (v/v) human serum (Sigma Aldrich) and 0.25% (w/v)
174 saponin. Cells were incubated with primary antibodies against STING, BTK, phospho-BTK-Y551 (all
175 from Cell Signaling Technology, 1:1000), DDX41 (Cell Signaling Technology, 1:1,000), and STING
176 (MilliporeSigma, 1:1,000) in 10% (v/v) human serum and 0.25% (w/v) saponin for 1 h at room
177 temperature. Following this, the cells were washed three times with 0.25% (w/v) saponin and incubated
178 with Alexa-488-conjugated anti-mouse and Alexa-647-conjugated anti-rabbit secondary antibodies
179 (both from Thermo Fisher, 1:1,000) for 1 h at room temperature, shielded from light. Finally, coverslips
180 were mounted with FluorSave reagent (MilliporeSigma) onto slides and visualized using a Leica SP8
181 inverted confocal microscope with a 63x oil immersion objective.

182 *Co-immunoprecipitation*

183 Cells were lysed in 1.0 ml of immunoprecipitation (IP) buffer [25 mM Tris, pH 7.4; 1 mM $MgCl_2$; 2 mM
184 EDTA; 1.0% Triton-X 100; 150 mM NaCl; Complete Protease Inhibitor Cocktail (Roche)] on ice for 2 h.
185 Protein G beads (100 µl; Protein G-sepharose Fast Flow, MilliporeSigma) were washed twice with IP
186 buffer (500 x *g*, 5 min), blocked for 1 h in 5.0% BSA in IP buffer, and then resuspended in 1 ml IP buffer.
187 The samples were clarified by centrifugation (12,000 x *g*, 10 min, 4°C), and 50 µl of the sample was
188 retained as the "input" control. Samples were incubated overnight at 4°C with protein G beads and 2 µg
189 of the precipitating antibody. The next day, the samples were centrifuged at 500 x *g* for 5 min, and 50
190 µl was reserved as the "unbound" sample. The samples were then washed four times with IP wash
191 buffer [25 mM Tris, pH 7.4; 10 mM $MgCl_2$; 2 mM EDTA; 0.1% Triton-X 100], with 50 µL retained after
192 washes 1 and 4. After the final wash, proteins in all samples were denatured using 2X SDS and heating
193 at 95°C for 10 min. The samples were then separated by SDS-PAGE and transferred to nitrocellulose
194 as described above.

195 *Toxicity Assay*

196 NuFF-1 cells (1.75 x 10^4 cells/well) were plated onto 96-well opaque white CulturPlate (Perkin
197 Elmer) and allowed to adhere overnight. Cells were then treated with orelabrutinib (GLPBio) in nine two-
198 fold dilutions (0.078 to 20 µM) for 24 h, followed by three washes with 1X PBS. Cell viability was
199 assessed after 2 and 5 days (i.e., 3 and 6 days post-treatment) using CellTiter-Glo (Promega) according
200 to the manufacturer's guidelines, and the plates were read with a Cytation 5 (Agilent) plate reader.
201 DMSO (equivalent v/v) served as the diluent and vehicle control, while puromycin (ranging from 20 µM
202 to 0.08 µM) was used as a positive control.

203 *Quantification of viral lytic replication*

204 NuFF-1 cells were treated with 0.5 µM orelabrutinib (GLPBio) prior to infection with TB40/E*mCherry*
205 (MOI = 0.01 $TCID_{50}$/cell) for 1 h, with gentle agitation every 15 min. After adsorption, cells were washed
206 three times with 1X PBS, and fresh media (V_f = 2.0 ml) containing 0.5 µM Orelabrutinib was added.
207 Cell-free virus (350 µl) was collected over a 16 day (d) timecourse, and 250 µl of fresh media with 100
208 µl of 10 µM orelabrutinib was added to restore the total volume to 2 ml. DMSO (equivalent v/v) served
209 as the diluent and vehicle control. Cell-associated virus was harvested at the final time point (16 days
210 post-infection; dpi) by lysing the cells through three freeze-thaw cycles. The clarified supernatant was
211 then used to determine the cell-assocated viral titer. Cell-free and cell-associated virus were quantified
212 by $TCID_{50}$ assay on naïve NuFF-1 fibroblasts.

213

214 **Results**

215 *BTK-DDX41-STING signaling is activated during lytic CMV infection*

216 Emerging data reveals an antiviral role for DDX41 (19, 28-30), though whether DDX41 functions as a
217 restriction factor during CMV infection remains unclear. To begin to address this, we first assessed the
218 expression of restriction factors associated with the BTK-DDX41-STING signaling pathway during lytic
219 CMV replication. We mock- or lytically-infected NuFF-1 fibroblasts with TB40/E*mCherry* (wild type; WT)
220 for 96 h, after which we measured protein abundance of the restriction factors, BTK, STING, DDX41
221 and TBK1, as well as the viral protein, IE1. We also quantified mRNA expression of *IFNB*, which
222 encodes IFN-β, a protein upregulated in response to innate immune signals. We found that infection
223 induces a time-dependent increase in protein expression of all restriction factors tested (**Fig. 1A**), as
224 well as *IFNB* transcription (**Fig. 1B**), consistent with previous findings for STING and IFN-β (31). While
225 abundance of the restriction factors increases over time, the timing varies among the factors, ranging
226 from as early as 6 h (DDX41) to 72 h (TBK1). STING expression does not show noticeable fluctuations
227 during infection; rather, it is upregulated early and its increased abundance is sustained throughout the
228 time course we evaluated (**Fig 1A**). These data indicate CMV induces an increase of BTK, STING,
229 DDX41, and TBK1 abundance, which results in increased *IFNB* expression in infected fibroblasts.

230 To investigate the signaling mechanism and confirm pathway activation, we used
231 immunofluorescence assays (IFA) to examine colocalization and coimmunoprecipitation to assess
232 interactions among restriction factors, with a particular focus on STING. Previous studies have shown
233 STING physically interacts with many of its signaling partners, such as TBK1 and IRF3, bringing them
234 into close proximity for phosphorylation and subsequent activation (32). We mock- or WT-infected
235 NuFF-1 fibroblasts for 96 h and visualized colocalization of each restriction factor (BTK, pBTK-Y551,
236 DDX41 and TBK) with STING by immunoflourescence. We observed BTK (**Fig. 2A**), its activated form
237 pBTK-Y551 (**Fig. 2B**), DDX41 (**Fig. 2C**), and TBK1 (**Fig. 2D**) each colocalize with STING at the
238 perinuclear region of the infected cell. Further, we confirmed the interaction between STING and BTK
239 (**Fig. 3A**), as well as STING and DDX41 (**Fig. 3B**) by co-immunoprecipitation, consistent with previous
240 findings (20, 33). As phosphorylation of these restriction factors is essential for their activation (20, 34-
241 36), we next assessed this post-translational modification on tyrosine residues in BTK, DDX41, and
242 STING. To this end, we WT-infected NuFF-1 fibroblasts for 96 h and confirmed phosphorylation through
243 immunoprecipitation with a phospho-tyrosine antibody. We then probed the immunoprecipitates for BTK
244 (**Fig. 4A**), DDX41 (**Fig. 4B**), and STING (**Fig. 4C**). Our data reveal phosphorylation of each of these
245 restriction factors following WT infection (**Fig 4**), suggesting that these restriction factors are activated
246 as part of the immune response against lytic CMV infection.

247

248 *CMV redistributes a fraction of DDX41 to the cytoplasm*

249 Our data reveal CMV infection results in distinct changes in the subcellular localization of the restriction
250 factors, including DDX41 (**Fig. 2**). In the absence of infection (mock control), DDX41 primarily displays
251 nuclear localization; however, CMV infection results in the progressive migration of this host restriction
252 factor to the perinuclear region (**Fig. 2**), consistent with previous work (19). Further, the CMV-induced
253 perinuclear relocalization of DDX41 suggested to us that this host protein may become co-localized
254 within the CMV vAC. To test this, we infected fibroblasts with a recombinant virus, TB40/E*mCherry*-
255 UL99*gfp*, that contains eGFP fused to the carboxy terminus of the *UL99* ORF (22, 23). *UL99* encodes
256 pp28, a viral protein that localizes to the vAC during lytic infection (37), which we also confirmed (**Fig.**
257 **5A**). Similar to our data in **Fig. 2**, we noted a portion of DDX41 relocalizes to the vAC (**Fig. 5A**).
258 Additionally, the other DDX41-associated restriction factors (BTK, STING, TBK1) also relocalize to the
259 vAC following CMV lytic infection (**Fig. S1**).To gain a better understanding of the abundance of DDX41
260 that was relocalized in response to CMV infection, we analyzed protein lysates derived from nuclear
261 and cytoplasmic fractions of mock- or WT-infected cells over a time course of infection. In mock-infected
262 cells, DDX41 retains its nuclear localization. However, in CMV-infected fibroblasts, a portion of DDX41
263 is translocated to the cytoplasm as early as 24 hpi, which persists through the time course we evaluated
264 (**Fig. 5B**). We hypothesized that since DDX41 is a dsDNA sensor, perhaps a portion of DDX41 is
265 retained within the nucleus by the host cell to target the viral genome. To test this, we evaluated whether
266 DDX41 colocalizes with the CMV DNA polymerase subunit, UL44, which we used to identify sites of
267 viral genome replication by IFA. Although a fraction of DDX41 remains in the nucleus during infection,
268 nuclear DDX41 does not specifically colocalize with UL44 (**Fig. 5C**), suggesting DDX41 does not sense
269 nuclear CMV DNA at the time point tested. Nonetheless, these results indicate a portion of DDX41 is
270 relocalized from the nucleus to the perinuclear region of the cytoplasmic vAC.

271 In addition to relocalizing this antiviral protein, we hypothesized that CMV infection may also
272 result in altered activity of the cytoplasmic portion of DDX41. Thus, we next asked whether perinuclear-
273 localized DDX41 exhibited altered signaling potency compared to its nuclear counterpart. To this end,
274 we analyzed the tyrosine phosphorylation of DDX41 in nuclear and cytoplasmic fractions of cells that
275 were either mock- or WT-infected, first confiming the fractionation using tubulin and H3 as cytoplasmic
276 and nuclear loading controls, respectively (**Fig. 6A**). We then performed immunoprecipitation with a
277 phospho-tyrosine antibody and probed for DDX41 in these fractions. Under mock conditions, DDX41 is
278 localized to the nucleus, consistent with our findings above, where it is phosphorylated. During infection,
279 although total DDX41 is more abundant in the cytoplasm than in the nucleus, the
280 phosphorylated/activated fraction in the cytoplasm is greatly reduced, as indicated by a reduction in the

281 p-Tyr DDX41 pulldown from the cytoplasmic fraction (**Fig. 6B**). Taken together, these data indicate
282 CMV infection induces a relocalization of a fraction of the inactivated form of DDX41 to the cytoplasm.

283 *DDX41 interacts with CMV-encoded tegument proteins*

284 Previous reports have noted a similar CMV-induced perinuclear distribution of the dsDNA sensor, IFI16.
285 At later stages of infection, IFI16 is localized to the vAC, where it interacts with the tegument protein,
286 pp65, to collectively subvert IFI16-mediated DNA sensing (10, 13, 18). Indeed, pp65 also interacts with
287 cGAS, thereby interfering with cGAS-STING interaction and innate sensing activity (10). In parallel,
288 *UL82*-encoded tegument protein, pp71, interacts with host restriction factors, ultimately preventing the
289 proper assembly of the STING-TBK1-IRF complex, whose activity is required for innate sensing via this
290 pathway (38). We therefore hypothesized that a similar interaction between CMV-encoded tegument
291 proteins and DDX41 regulates this host restriction factor's localization and activity. To this end, we
292 infected fibroblasts and assessed the potential co-localization and interaction between DDX41 and
293 either pp65 or pp71. Our findings reveal DDX41 co-localizes with pp65 (**Fig. 7A**) and pp71 (**Fig. 7B**) in
294 the perinuclear vAC. Further, DDX41 interacts with pp65 (**Fig. 7C**) as well pp71, though detection of
295 this latter interaction is far weaker than the former (**Fig. 7D**). These results suggest that pp65, and to a
296 lesser extent, pp71, interact with DDX41, likely retaining this host restriction factor in the cytoplasmic
297 vAC.

298 *Activated BTK-DDX41-dependent STING signaling limits CMV protein expression and replication*

299 Since our data indicate BTK, DDX41, and STING are activated during lytic CMV infection, we next
300 assessed the contribution of this branch of STING signaling during infection. To this end, we utilized
301 pharmacological inhibition using orelabrutinib, a highly specific and irreversible BTK inhibitor (39). Since
302 BTK activates DDX41 (20), we posited this would serve as a reasonable approach to inhibit DDX41, as
303 our attempts of both knockout and knockdown of this protein were unsuccessful (data not shown). This
304 is perhaps not surprising, as DDX41 is embryonic lethal (40). Using the pharmacological approach
305 instead, we first evaluated the toxicity and efficacy of orelabrutinib in our model system and observed
306 minimal toxicity over a concentration range of 0.078 to 20 μM. To validate the assay, we included
307 puromycin treatment as a positive control (**Fig. S2A**). We also evaluated the impact of orelabrutinib
308 treatment on the signaling pathway using a multipronged approach. We assessed DDX41 protein
309 abundance following orelabrutinib treatment at various concentrations (0.1–10 μM) and durations (24–
310 120 h at 0.5 μM). DDX41 abundance was attenuated following 0.5 μM orelabrutinib treatment, which
311 was further decreased with increasing concentration of orelabrutinib (**Fig. S2B**) and longer treatment
312 times (**Fig. S2C**). Additionally, orelabrutinib treatment reduced *IFNB* transcription in WT-infected cells,
313 although this reduction was not statistically significant (**Fig. S2D**). Despite this, we did observe

314 diminished phosphorylation of BTK (**Figs. S3A**) and DDX41 (**Figs. S3B**) in orelabrutinib-treated, WT-
315 infected cells compared to untreated counterpart cultures in IP-western assays (**Fig. S3**) . Our data also
316 reveal orelabrutinib-treated, WT-infected cells display a reduction in total DDX41 abundance (**Fig. S3B**),
317 which likely also contributes to attenuated phosphorylation levels of this protein. Collectively, these data
318 suggest that orelabrutinib inhibit BTK and DDX41 activity without causing toxicity in fibroblasts.

319 Having an effective means by which to target DDX41, we leveraged orelabrutinib to assess the
320 impact of inhibiting BTK-DDX41-dependent STING signaling on lytic CMV infection. To this end, to
321 determine the impact of orelabrutinib-mediated DDX41 inhibition on viral protein translation, we
322 evaluated the abundance of representative viral proteins from the early and late kinetic classes.
323 Orelabrutinib-treated, WT-infected cells displayed a reduction in the expression of BTK, DDX41, and
324 STING compared to infected cells treated with DMSO (-orelabrutinib, **Fig 8A**). Concurrent with the
325 reduced abundance of these restriction factors, we observed increased abundance of the viral early
326 protein, UL44, and the viral late protein, pp65 (**Fig. 8A**). In parallel, we treated fibroblasts with 0.5 μM
327 orelabrutinib and infected the cells with WT virus at (MOI = 0.01 $TCID_{50}$/cell) over a 16-day time course.
328 Our multistep growth analysis of cell-free virus production revealed orelabrutinib treatment resulted in
329 an increase in CMV replication from 8 – 16 dpi, with a statistically significant increase at 12 dpi (**Fig.
330 8B**). Additionally, cell-associated virus also increased in the presence of orelabrutinib, although not to
331 statistically significant levels (**Fig. 8C**). In sum, these data show that attenuation of BTK-DDX41-
332 dependent signaling promotes CMV lytic replication, indicating this branch of STING signaling plays a
333 protective role.

334 **Discussion**

335 Here we show BTK-DDX41-dependent STING signaling functions in the innate immune response
336 against lytic CMV infection. Specifically, our data reveal this branch of STING signaling is activated
337 through the interaction of BTK and DDX41 with STING (**Figs. 1-3**), along with the phosphorylation of
338 tyrosine residues on all three restriction factors (**Fig. 4**). Further, CMV infection induces a cytoplasmic
339 redistribution of DDX41 and its associated restriction factors to the perinuclear virus assembly
340 compartment (vAC; **Fig. 5**), where it interacts with the CMV tegument proteins pp65 and pp71 (**Fig. 7**).
341 In the cytoplasm, DDX41 exhibits reduced activation, as evidenced by decreased tyrosine
342 phosphorylation (**Fig. 6**). Additionally, we demonstrate the protective nature of this signaling pathways
343 by pharmacological inhibition of BTK using orelabrutinib, an inhibitor that attenuates this signaling axis
344 and results in increased viral protein abundance and CMV replication (**Fig. 8**). Collectively, our findings
345 underscore the significance of this signaling pathway and reveal a mechanism by which CMV evades
346 the immune response.

347 dsDNA sensors are of considerable interest in the context of CMV, as several, including cGAS,
348 IFI16, AIM2, and ZBP1, trigger IFN production upon detection of the CMV genome (41-44). Our findings
349 herein now add DDX41 to this growing repertoire of sensors that are involved in the innate response
350 against CMV. Our study shows that lytic CMV infection induces the abundance of BTK, DDX41, STING,
351 and TBK1, as well as accumulation of *IFNB* transcripts. We confirmed the activation of the pathway, as
352 evidenced by the phosphorylation of BTK, DDX41 and STING, with both BTK and DDX41 colocalizing
353 and interacting with STING. Previous research showed DDX41 interacts with STING at its second to
354 fourth transmembrane domains in poly(dA)-stimulated myeloid dendritic cells (28). Additionally, in a
355 HEK293T-based overexpression system, the BTK SH3/SH2-interaction domain binds the
356 transmembrane region of STING (20). This mediatory role of STING is well-documented; for example,
357 STING interacts with TBK1 and IRF3, and then facilitates the phosphorylation and activation of IRF3 by
358 TBK1 (32). We hypothesize a similar mechanism based on the results from our study - after BTK and
359 DDX41 bind STING, BTK could activate DDX41 through phosphorylation. Although it remains unclear
360 whether STING directly induces this phosphorylation or merely facilitates the proximity of BTK and
361 DDX41, current data suggest STING likely plays a more active role in the process.

362 Multiple studies have highlighted CMV's diverse mechanisms to counteract DNA sensor-
363 dependent immunity at various levels. At the DNA sensing level, CMV UL31 interacts with cGAS,
364 causing the dissociation of DNA from cGAS and negatively regulating the STING signaling pathway
365 (11). Similarly, UL42 binds cGAS, in turn inhibiting its DNA binding, oligomerization, and enzymatic
366 activity (12). The tegument protein, pp65, also binds cGAS, preventing its interaction with STING and
367 thus inactivating STING signaling (10). pp65 also interacts with IFI16's PYRIN domain, blocking its
368 oligomerization upon DNA sensing and subsequent immune signaling (14). This propensity of viral
369 proteins, particularly pp65, to bind dsDNA sensors, drew our attention to tegument proteins and their
370 potential interaction with DDX41. Indeed, we found DDX41 associates with both pp65 and, to a lesser
371 extent, pp71 during lytic CMV infection. The decreased detection of pp71 does not necessarily imply a
372 weaker or less probable interaction, but rather could result from diminished availability of pp71 for
373 interaction with DDX41 compared to pp65.

374 What remains outstanding is whether the interaction between DDX41 and pp65 and/or pp71 is
375 required for relocalizing DDX41 to the vAC. While possible, it is unlikely the tegument proteins aid in
376 DDX41 redistribution. Others have reported DDX41 relocalization to perinuclear regions in response to
377 DNA stimuli (19, 45), which Singh and colleagues demonstrated is dependent upon acetylation of
378 DDX41's most amino-terminal nuclear localization signal (NLS; (19)). It is thus likely that DDX41
379 cytoplasmic localization during CMV infection is stimulated in a similar fashion, dependent upon DNA
380 sensing, as opposed to specific, CMV-encoded factors. Why would CMV-encoded tegument proteins

interact with vAC-localized DDX41? It is possible the tegument proteins interact with DDX41 to retain this host protein in a less active state late in infection. We showed cytoplasmic DDX41 activity is attenuated, despite its colocalization with STING and BTK in the perinuclear region. It is attractive to hypothesize that the interaction with the tegument proteins precludes DDX41 activation, similar to what is reported for cGAS and IFI16 (10, 14). Alternatively, perhaps the CMV tegument protein(s)-DDX41 interaction results in DDX41's incorporation into the mature viral particle, similar to that reported for IFI16 (18). This could ensure DDX41 is delivered to newly infected cells, allowing for its immediate action for very early innate responses following infection. This latter hypothesis could support the basis for the more late-phase phenotypes we observed herein. Further, virion-delivered DDX41 may indicate additional functions beyond innate immune responses, similar to IFI16, which also interacts with pp65 to activate viral gene transcription at the major immediate early promoter (14). DDX41 may have additional functions during CMV infection, as this host protein additionally coordinates RNA splicing and transcriptional elongation, thereby preventing DNA replication stress (46). Thus, one could posit DDX41's functions during CMV infection are more extensive, raising the possibility its potential inclusion in the virion serves a biologically important purpose. These are compelling questions warranting further exploration, and experiments to address these possibilities are on-going.

Our findings herein highlight the protective role of BTK-DDX41-dependent STING signaling in the immune response to CMV lytic infection and further reveals a mechanism of immune evasion through disrupted activation and localization of DDX41. Our work advances our understanding of innate responses against CMV, providing insights that could inform strategies to counteract CMV's immune evasive strategies.

Acknowledgements

The authors thank Ian Groves for helpful discussions and Ganes Sen for critical reading of the manuscript. The authors also thank Amanda Mendelsohn (Cleveland Clinic Enterprise Creative Services) for assistance with the graphical image.

Funding

This work was supported in part by the National Institutes of Health Core Instrument award (S10OD019972; awarded to Judy Drazba, Director, Cleveland Clinic Imaging Core).

References

1. Griffiths P, Reeves M. 2021. Pathogenesis of human cytomegalovirus in the immunocompromised host. Nat Rev Microbiol 19:759-773.

415 2. Smith NA, Chan GC, O'Connor CM. 2021. Modulation of host cell signaling during cytomegalovirus
416 latency and reactivation. Virol J 18:207.
417 3. Antinori A, Bausch-Jurken M. 2023. The Burden of COVID-19 in the Immunocompromised Patient:
418 Implications for Vaccination and Needs for the Future. J Infect Dis 228:S4-S12.
419 4. Martinson ML, Lapham J. 2024. Prevalence of Immunosuppression Among US Adults. JAMA 331:880-
420 882.
421 5. Jones CE, Bailey H, Bamford A, Calvert A, Dorey RB, Drysdale SB, Khalil A, Heath PT, Lyall H, Ralph
422 KMI, Sapuan S, Vandrevala T, Walter S, Whittaker E, Wood S, Collaboration UKCCI. 2023. Managing
423 challenges in congenital CMV: current thinking. Arch Dis Child 108:601-607.
424 6. Boppana SB, Ross SA, Fowler KB. 2013. Congenital cytomegalovirus infection: clinical outcome. Clin
425 Infect Dis 57 Suppl 4:S178-81.
426 7. Dell'Oste V, Biolatti M, Galitska G, Griffante G, Gugliesi F, Pasquero S, Zingoni A, Cerboni C, De
427 Andrea M. 2020. Tuning the Orchestra: HCMV vs. Innate Immunity. Front Microbiol 11:661.
428 8. Marques M, Ferreira AR, Ribeiro D. 2018. The Interplay between Human Cytomegalovirus and
429 Pathogen Recognition Receptor Signaling. Viruses 10.
430 9. Almine JF, O'Hare CA, Dunphy G, Haga IR, Naik RJ, Atrih A, Connolly DJ, Taylor J, Kelsall IR, Bowie
431 AG, Beard PM, Unterholzner L. 2017. IFI16 and cGAS cooperate in the activation of STING during DNA
432 sensing in human keratinocytes. Nat Commun 8:14392.
433 10. Biolatti M, Dell'Oste V, Pautasso S, Gugliesi F, von Einem J, Krapp C, Jakobsen MR, Borgogna C,
434 Gariglio M, De Andrea M, Landolfo S. 2018. Human Cytomegalovirus Tegument Protein pp65 (pUL83)
435 Dampens Type I Interferon Production by Inactivating the DNA Sensor cGAS without Affecting STING. J
436 Virol 92.
437 11. Huang ZF, Zou HM, Liao BW, Zhang HY, Yang Y, Fu YZ, Wang SY, Luo MH, Wang YY. 2018. Human
438 Cytomegalovirus Protein UL31 Inhibits DNA Sensing of cGAS to Mediate Immune Evasion. Cell Host
439 Microbe 24:69-80 e4.
440 12. Fu YZ, Guo Y, Zou HM, Su S, Wang SY, Yang Q, Luo MH, Wang YY. 2019. Human cytomegalovirus
441 protein UL42 antagonizes cGAS/MITA-mediated innate antiviral response. PLoS Pathog 15:e1007691.
442 13. Cristea IM, Moorman NJ, Terhune SS, Cuevas CD, O'Keefe ES, Rout MP, Chait BT, Shenk T. 2010.
443 Human cytomegalovirus pUL83 stimulates activity of the viral immediate-early promoter through its
444 interaction with the cellular IFI16 protein. J Virol 84:7803-14.
445 14. Li T, Chen J, Cristea IM. 2013. Human cytomegalovirus tegument protein pUL83 inhibits IFI16-mediated
446 DNA sensing for immune evasion. Cell Host Microbe 14:591-9.
447 15. Choi HJ, Park A, Kang S, Lee E, Lee TA, Ra EA, Lee J, Lee S, Park B. 2018. Human cytomegalovirus-
448 encoded US9 targets MAVS and STING signaling to evade type I interferon immune responses. Nat
449 Commun 9:125.
450 16. Nukui M, Roche KL, Jia J, Fox PL, Murphy EA. 2020. Protein S-Nitrosylation of Human Cytomegalovirus
451 pp71 Inhibits Its Ability To Limit STING Antiviral Responses. J Virol 94.
452 17. Albright ER, Mickelson CK, Kalejta RF. 2021. Human Cytomegalovirus UL138 Protein Inhibits the
453 STING Pathway and Reduces Interferon Beta mRNA Accumulation during Lytic and Latent Infections.
454 mBio 12:e0226721.
455 18. Dell'Oste V, Gatti D, Gugliesi F, De Andrea M, Bawadekar M, Lo Cigno I, Biolatti M, Vallino M,
456 Marschall M, Gariglio M, Landolfo S. 2014. Innate nuclear sensor IFI16 translocates into the cytoplasm
457 during the early stage of in vitro human cytomegalovirus infection and is entrapped in the egressing
458 virions during the late stage. J Virol 88:6970-82.
459 19. Singh RS, Vidhyasagar V, Yang S, Arna AB, Yadav M, Aggarwal A, Aguilera AN, Shinriki S,
460 Bhanumathy KK, Pandey K, Xu A, Rapin N, Bosch M, DeCoteau J, Xiang J, Vizeacoumar FJ, Zhou Y,
461 Misra V, Matsui H, Ross SR, Wu Y. 2022. DDX41 is required for cGAS-STING activation against DNA
462 virus infection. Cell Rep 39:110856.
463 20. Lee KG, Kim SS, Kui L, Voon DC, Mauduit M, Bist P, Bi X, Pereira NA, Liu C, Sukumaran B, Renia L,
464 Ito Y, Lam KP. 2015. Bruton's tyrosine kinase phosphorylates DDX41 and activates its binding of
465 dsDNA and STING to initiate type 1 interferon response. Cell Rep 10:1055-65.
466 21. O'Connor CM, Shenk T. 2011. Human cytomegalovirus pUS27 G protein-coupled receptor homologue
467 is required for efficient spread by the extracellular route but not for direct cell-to-cell spread. J Virol
468 85:3700-7.
469 22. Nukui M, O'Connor CM, Murphy EA. 2018. The Natural Flavonoid Compound Deguelin Inhibits HCMV
470 Lytic Replication within Fibroblasts. Viruses 10.

471 23. O'Connor CM, Nukui M, Gurova KV, Murphy EA. 2016. Inhibition of the FACT Complex Reduces
472 Transcription from the Human Cytomegalovirus Major Immediate Early Promoter in Models of Lytic and
473 Latent Replication. J Virol 90:4249-4253.
474 24. O'Connor CM, Shenk T. 2012. Human cytomegalovirus pUL78 G protein-coupled receptor homologue is
475 required for timely cell entry in epithelial cells but not fibroblasts. J Virol 86:11425-33.
476 25. Zhu H, Shen Y, Shenk T. 1995. Human cytomegalovirus IE1 and IE2 proteins block apoptosis. J Virol
477 69:7960-70.
478 26. Bechtel JT, Shenk T. 2002. Human cytomegalovirus UL47 tegument protein functions after entry and
479 before immediate-early gene expression. J Virol 76:1043-50.
480 27. Schneider CA, Rasband WS, Eliceiri KW. 2012. NIH Image to ImageJ: 25 years of image analysis. Nat
481 Methods 9:671-5.
482 28. Zhang Z, Yuan B, Bao M, Lu N, Kim T, Liu YJ. 2011. The helicase DDX41 senses intracellular DNA
483 mediated by the adaptor STING in dendritic cells. Nat Immunol 12:959-65.
484 29. Stavrou S, Aguilera AN, Blouch K, Ross SR. 2018. DDX41 Recognizes RNA/DNA Retroviral Reverse
485 Transcripts and Is Critical for In Vivo Control of Murine Leukemia Virus Infection. mBio 9.
486 30. Duan Y, Zeng J, Fan S, Liao Y, Feng M, Wang L, Zhang Y, Li Q. 2019. Herpes Simplex Virus Type 1-
487 Encoded miR-H2-3p Manipulates Cytosolic DNA-Stimulated Antiviral Innate Immune Response by
488 Targeting DDX41. Viruses 11.
489 31. Lio CW, McDonald B, Takahashi M, Dhanwani R, Sharma N, Huang J, Pham E, Benedict CA, Sharma
490 S. 2016. cGAS-STING Signaling Regulates Initial Innate Control of Cytomegalovirus Infection. J Virol
491 90:7789-97.
492 32. Tanaka Y, Chen ZJ. 2012. STING specifies IRF3 phosphorylation by TBK1 in the cytosolic DNA
493 signaling pathway. Sci Signal 5:ra20.
494 33. Parvatiyar K, Zhang Z, Teles RM, Ouyang S, Jiang Y, Iyer SS, Zaver SA, Schenk M, Zeng S, Zhong W,
495 Liu ZJ, Modlin RL, Liu YJ, Cheng G. 2012. The helicase DDX41 recognizes the bacterial secondary
496 messengers cyclic di-GMP and cyclic di-AMP to activate a type I interferon immune response. Nat
497 Immunol 13:1155-61.
498 34. Rawlings DJ, Scharenberg AM, Park H, Wahl MI, Lin S, Kato RM, Fluckiger AC, Witte ON, Kinet JP.
499 1996. Activation of BTK by a phosphorylation mechanism initiated by SRC family kinases. Science
500 271:822-5.
501 35. Wang C, Wang X, Veleeparambil M, Kessler PM, Willard B, Chattopadhyay S, Sen GC. 2020. EGFR-
502 mediated tyrosine phosphorylation of STING determines its trafficking route and cellular innate immunity
503 functions. EMBO J 39:e104106.
504 36. Wang C, Sharma N, Veleeparambil M, Kessler PM, Willard B, Sen GC. 2021. STING-Mediated
505 Interferon Induction by Herpes Simplex Virus 1 Requires the Protein Tyrosine Kinase Syk. mBio
506 12:e0322821.
507 37. Sanchez V, Sztul E, Britt WJ. 2000. Human cytomegalovirus pp28 (UL99) localizes to a cytoplasmic
508 compartment which overlaps the endoplasmic reticulum-golgi-intermediate compartment. J Virol
509 74:3842-51.
510 38. Fu YZ, Su S, Gao YQ, Wang PP, Huang ZF, Hu MM, Luo WW, Li S, Luo MH, Wang YY, Shu HB. 2017.
511 Human Cytomegalovirus Tegument Protein UL82 Inhibits STING-Mediated Signaling to Evade Antiviral
512 Immunity. Cell Host Microbe 21:231-243.
513 39. Dhillon S. 2021. Orelabrutinib: First Approval. Drugs 81:503-507.
514 40. Badar T, Chlon T. 2022. Germline and Somatic Defects in DDX41 and its Impact on Myeloid
515 Neoplasms. Curr Hematol Malig Rep 17:113-120.
516 41. Paijo J, Doring M, Spanier J, Grabski E, Nooruzzaman M, Schmidt T, Witte G, Messerle M, Hornung V,
517 Kaever V, Kalinke U. 2016. cGAS Senses Human Cytomegalovirus and Induces Type I Interferon
518 Responses in Human Monocyte-Derived Cells. PLoS Pathog 12:e1005546.
519 42. Gariano GR, Dell'Oste V, Bronzini M, Gatti D, Luganini A, De Andrea M, Gribaudo G, Gariglio M,
520 Landolfo S. 2012. The intracellular DNA sensor IFI16 gene acts as restriction factor for human
521 cytomegalovirus replication. PLoS Pathog 8:e1002498.
522 43. Huang Y, Ma D, Huang H, Lu Y, Liao Y, Liu L, Liu X, Fang F. 2017. Interaction between HCMV pUL83
523 and human AIM2 disrupts the activation of the AIM2 inflammasome. Virol J 14:34.
524 44. DeFilippis VR, Alvarado D, Sali T, Rothenburg S, Fruh K. 2010. Human cytomegalovirus induces the
525 interferon response via the DNA sensor ZBP1. J Virol 84:585-98.
526 45. Ma JX, Li JY, Fan DD, Feng W, Lin AF, Xiang LX, Shao JZ. 2018. Identification of DEAD-Box RNA
527 Helicase DDX41 as a Trafficking Protein That Involves in Multiple Innate Immune Signaling Pathways in
528 a Zebrafish Model. Front Immunol 9:1327.

46. Shinriki S, Hirayama M, Nagamachi A, Yokoyama A, Kawamura T, Kanai A, Kawai H, Iwakiri J, Liu R, Maeshiro M, Tungalag S, Tasaki M, Ueda M, Tomizawa K, Kataoka N, Ideue T, Suzuki Y, Asai K, Tani T, Inaba T, Matsui H. 2022. DDX41 coordinates RNA splicing and transcriptional elongation to prevent DNA replication stress in hematopoietic cells. Leukemia 36:2605-2620.

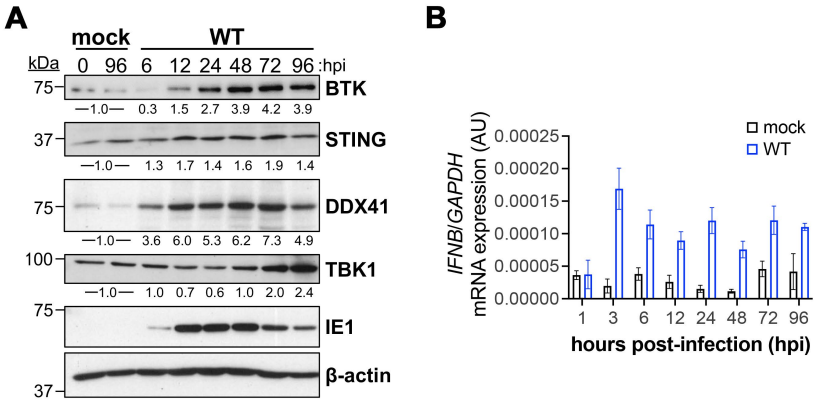

Figure 1. CMV infection induces a time-dependent increase in STING, DDX41, and TBK1 protein abundance, as well as *IFNB* mRNA expression. NuFF-1 fibroblasts were mock- or WT-infected (MOI = 0.5 $TCID_{50}$/cell). (**A**) At the indicated times post-infection, cells were collected and equal concentration (30 µg) of lysates were probed for cellular proteins, STING, DDX41, and TBK1, as well as the viral protein, IE1. Cellular β-actin was probed as a loading control. Protein expression was quantified by densitometry after normalization to an internal standard (β-actin), relative to mean signal from mock at 0 h and 96 h. N = 3, representative blots shown. (**B**) Total RNA was isolated at the indicated times post-infection, and *IFNB* was measured by RT-qPCR and plotted in arbitrary units (AU) as ΔΔCt relative to cellular *GAPDH*. All samples within a biological replicate were assessed in triplicate. N = 3, representative experiment shown.

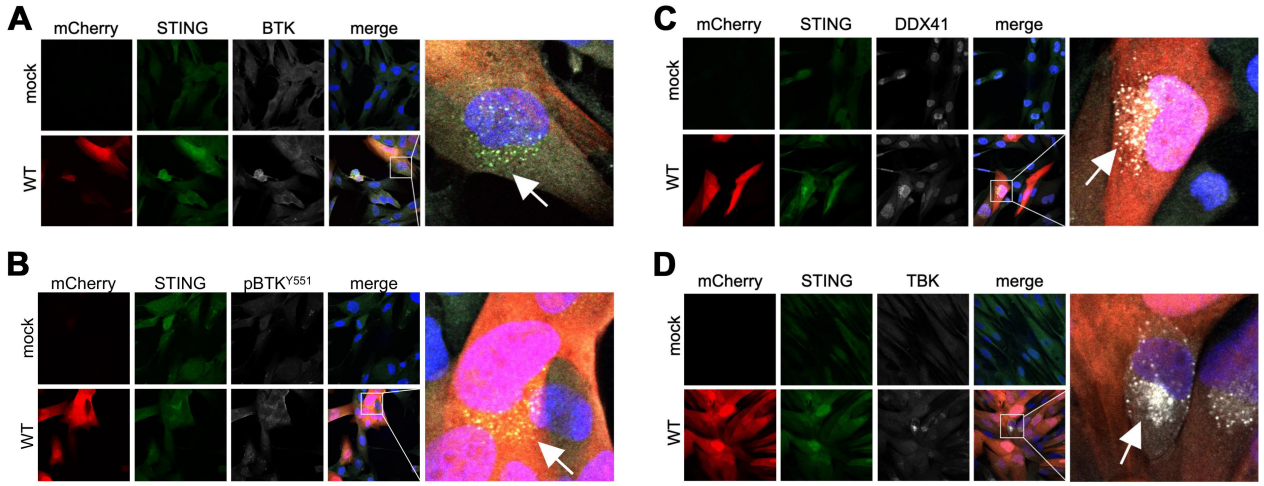

Figure 2. BTK, DDX41, and TBK1 co-localize with STING during CMV infection. NuFF-1 fibroblasts were mock- or WT-infected (MOI = 0.5 $TCID_{50}$/cell) for 96 h, after which cells were processed for immunofluorescence assay (IFA). Cells were then probed with antibodies directed at: (**A**) BTK, (**B**) pBTK-Y551, (**C**) DDX41, or (**D**) TBK1 (each shown in white), as well as (**A-D**) STING (green). mCherry (red) is a marker of lytic infection; nuclei were visualized with DAPI (blue). Inset in the WT merge panel is enlarged at right. Images were acquired using 63x objective. N = 3; representative images shown.

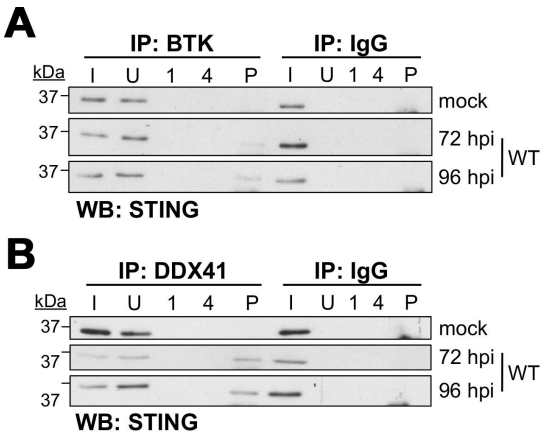

Figure 3. BTK and DDX41 interact with STING during CMV infection. NuFF-1 fibroblasts were mock- or WT-infected (MOI = 0.5 $TCID_{50}$/cell) for the indicated times. Cells were then harvested, and immunoprecipitated (IP) with antibodies specific for (**A**) BTK, (**B**) DDX41, or (**A,B**) IgG. Immunoprecipitates were then probed for STING by western blot (WB). I, input; U, unbound; 1, wash #1; 4, wash #4; P, IP sample. N = 3; representative blots shown.

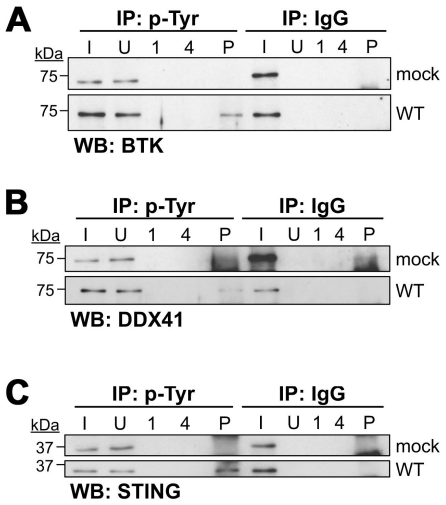

Figure 4. CMV infection results in activation of BTK, DDX41, and STING. NuFF-1 fibroblasts were either mock- or WT-infected (MOI = 0.5 $TCID_{50}$/cell). At 96 hours post-infection, cells were then harvested, and immunoprecipitated (IP) with antibodies specific for phosphorylated-Tyrosine (p-Tyr) or IgG. Immunoprecipitates were then probed for the following antibodies by western blot (WB): (**A**) BTK, (**B**) DDX41, or (**C**) STING. I, input; U, unbound; 1, wash #1; 4, wash #4; P, IP sample. N = 3; representative blots shown.

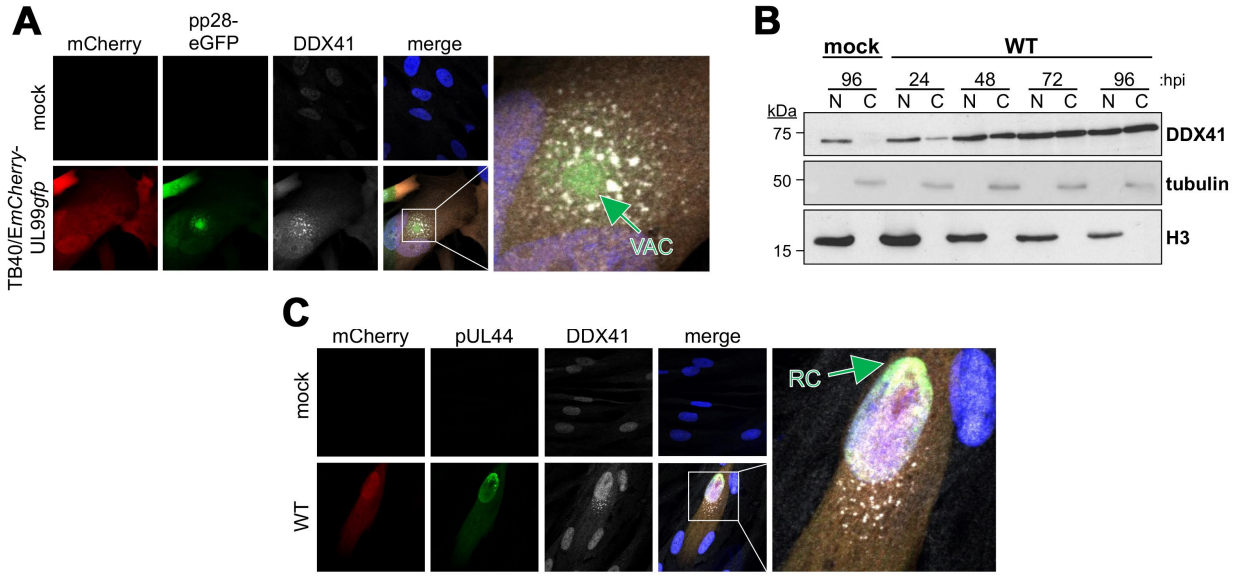

Figure 5. DDX41 is translocated from the nucleus to the perinuclear viral assembly compartment (VAC). (**A**) NuFF-1 fibroblasts were mock- or *UL99gfp*-infected (MOI = 0.5 $TCID_{50}$/cell) for 96 h. Cells were then fixed, permeabilized, and stained for DDX41 (white). mCherry (red) is a marker of lytic infection, pp28-eGFP is shown in green, and nuclei were visualized with DAPI (blue). VAC, viral assembly compartment. (**B**) NuFF-1 fibroblasts were mock- or WT-infected (MOI = 0.5 $TCID_{50}$/cell) for the indicated times. Lysates (20 µg) from nuclear (N) and cytoplasmic (C) fractions were probed for DDX41, tubulin (cytoplasmic marker), and histone H3 (nuclear marker). N = 3; representative blots shown. (**C**) NuFF-1 fibroblasts were infected as in (**B**) for 96 h. Following fixation and permeabilization, cells were stained for pUL44 (green) and DDX41 (white). mCherry (red) is a marker of lytic replication and DAPI (blue) was used to visualize nuclei. Viral replication compartment (RC) is indicated. (**A,C**) Images were acquired using 63x objective. N = 3; representative images shown.

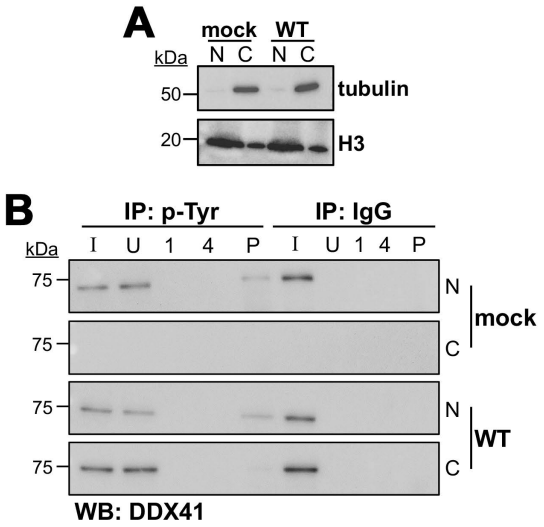

Figure 6. CMV-induced cytoplasmic DDX41 localization results in attenuated phosphorylation. NuFF-1 fibroblasts were mock- or WT-infected (MOI = 0.5 $TCID_{50}$/cell). At 96 hpi, cells were harvested and nuclear (N) and cytoplasmic (C) fractions isolated. (**A**) Nuclear (N) and cytoplasmic (C) fractions were probed for tubulin (cytoplasmic) or histone H3 (nuclear). (**B**) Fractions from (**A**) were then immunoprecipitated (IP) with antibodies specific phosphorylated Tyrosine (p-Tyr) or IgG and were then probed for DDX41 by western blot (WB). I, input; U, unbound; 1, wash #1; 4, wash #4; P, IP sample. N = 3; representative blots shown.

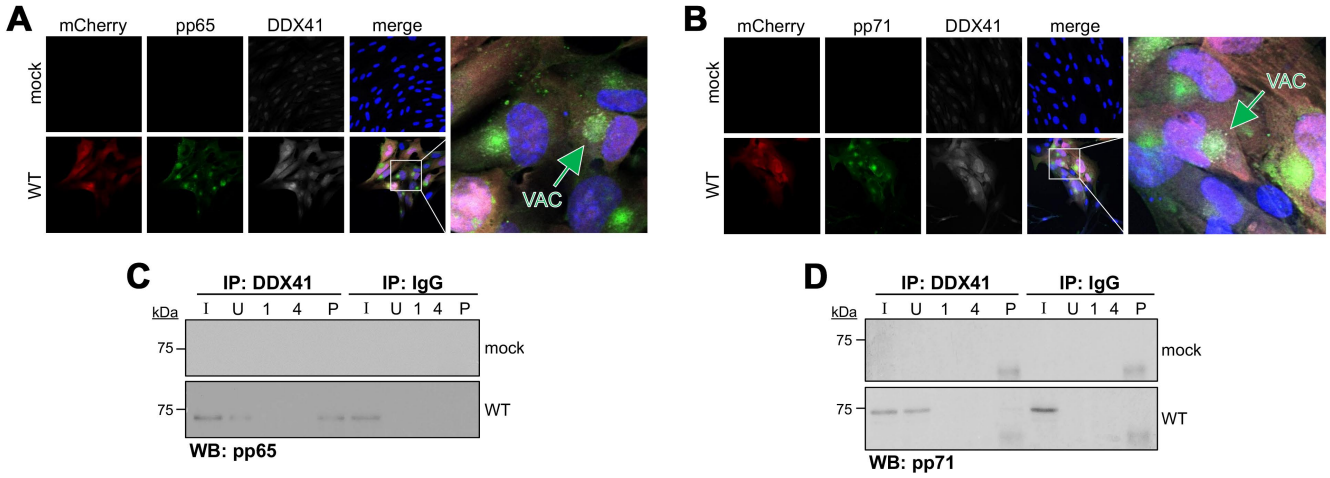

Figure 7. CMV tegument proteins, pp65 and pp71, interact with DDX41 and co-localize with DDX41 in the vAC. NuFF-1 fibroblasts were mock- or WT-infected (MOI = 0.5 $TCID_{50}$/cell) for 96 h. (**A,B**) Cells were fixed, permeabilized and stained for DDX41 (white) and either (**A**) pp65 (green) or (**B**) pp71 (green). (**A,B**) mCherry (red) is shown as a marker of infection, and nuclei were visualized with DAPI (blue). (**C,D**) Cells were then harvested, and proteins immunoprecipitated (IP) with antibodies specific for DDX41 or IgG. Immunoprecipitates were then probed for (**C**) pp65 or (**D**) pp71 by western blot (WB). (**C,D**) I, input; U, unbound; 1, wash #1; 4, wash #4; P, IP sample. N = 3; representative blots shown.

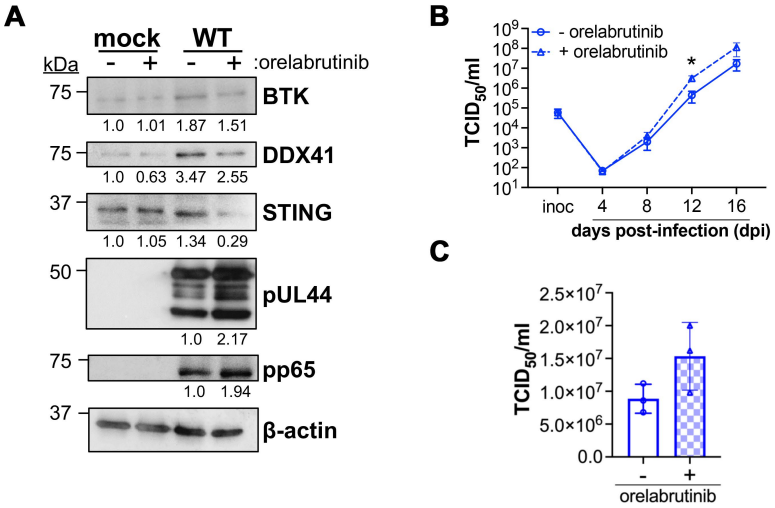

Figure 8. Orelabrutinib inhibition of BTK/DDX41 signaling induces lytic CMV infection. (**A**) NuFF-1 fibroblasts were pre-treated with 0.5 μM orelabrutinib (+ orelabrutinib) or DMSO (v/v; - orelabrutinib) for 1 h prior to mock or WT infection (MOI = 0.5 $TCID_{50}$/cell). At 96 hpi, cells were harvested and lysates (25 μg) probed for the indicated proteins. N = 3; representative blots shown. (**B,C**) NuFF-1 fibroblasts were treated with 0.5 μM orelabrutinib (+ orelabrutinib; open triangles) or DMSO (v/v; - orelabrutinib; open circles) for 1 h, and then infected with WT (MOI = 0.01 $TCID_{50}$/cell). Following adsorption, cells were washed and replenished with fresh media containing orelabrutinib (0.5 μM) or DMSO (v/v). (**B**) Cell-free virus was collected over a 16-day time course (- orelabrutinib, dashed line; + orelabrutinib, solid line), and (**C**) cell-associated virus was harvested at 16 dpi (- orelabrutinib, open bar; + orelabrutinib, checked bar). (**B,C**) Viral titers were quantified by $TCID_{50}$ using naïve NuFF-1 fibroblasts. Samples within a biological replicate were analyzed in triplicate. N = 3; representative experiment shown. Data are mean±s.d. of the technical replicates (datapoints). Statistical significance was calculated by paired t-test. Data are not significant unless otherwise noted; *$p < 0.05$.

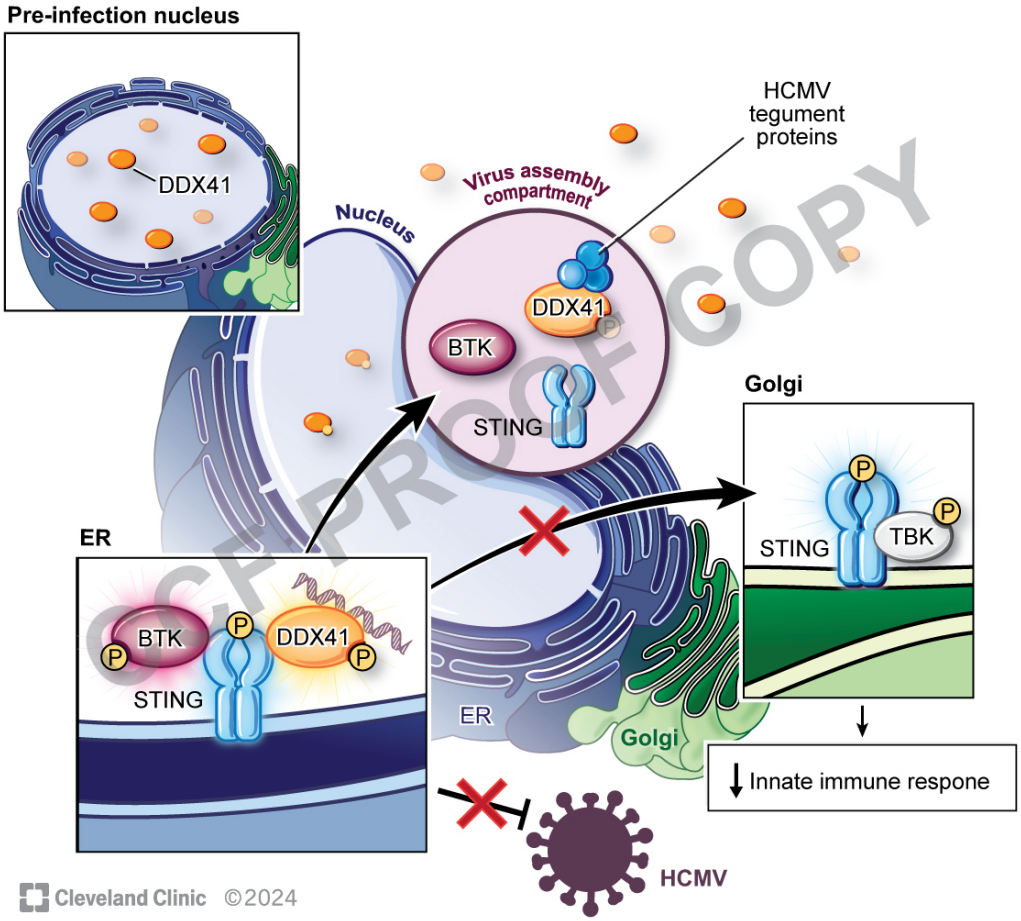

GCF PROOF COPY

Figure 9. Model depicting CMV-mediated displacement of host restriction factors, mitigating the protective DDX41/BTK/STING signaling axis. BTK/DDX41/STING signaling is protective against lytic CMV infection. CMV suppresses this signaling axis by displacing the restriction factors to the virus assembly complex, where DDX41 interacts with CMV tegument proteins. Cytoplasmic redistribution of these host restriction factors results in their decreased activity important for initiating antiviral signaling.

Supplemental Figures

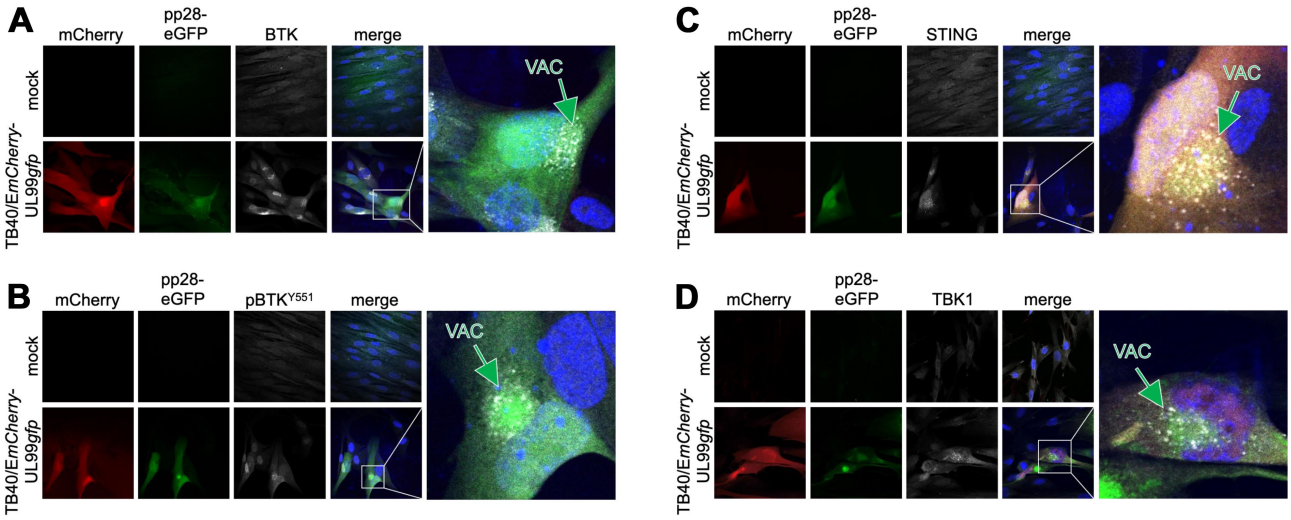

Figure S1. DDX41-associated restriction factors localize to the viral assembly compartment (VAC). NuFF-1 fibroblasts were mock- or TB40/E*mCherry*-UL99*gfp* (UL99*gfp*; MOI = 0.5 $TCID_{50}$/cell) for 96 h. Cells were then fixed, permeabilized, and probed for: (**A**) BTK, (**B**) $pBTK^{Y551}$, (**C**) STING or (**D**) TBK1 (each shown in white). (A-D) mCherry (red) is a marker of lytic infection, pp28-eGFP is shown in green, and nuclei were visualized with DAPI (blue). The viral assembly compartment (VAC) is denoted by the arrow. Images were acquired using 63x objective. N = 3; representative images shown.

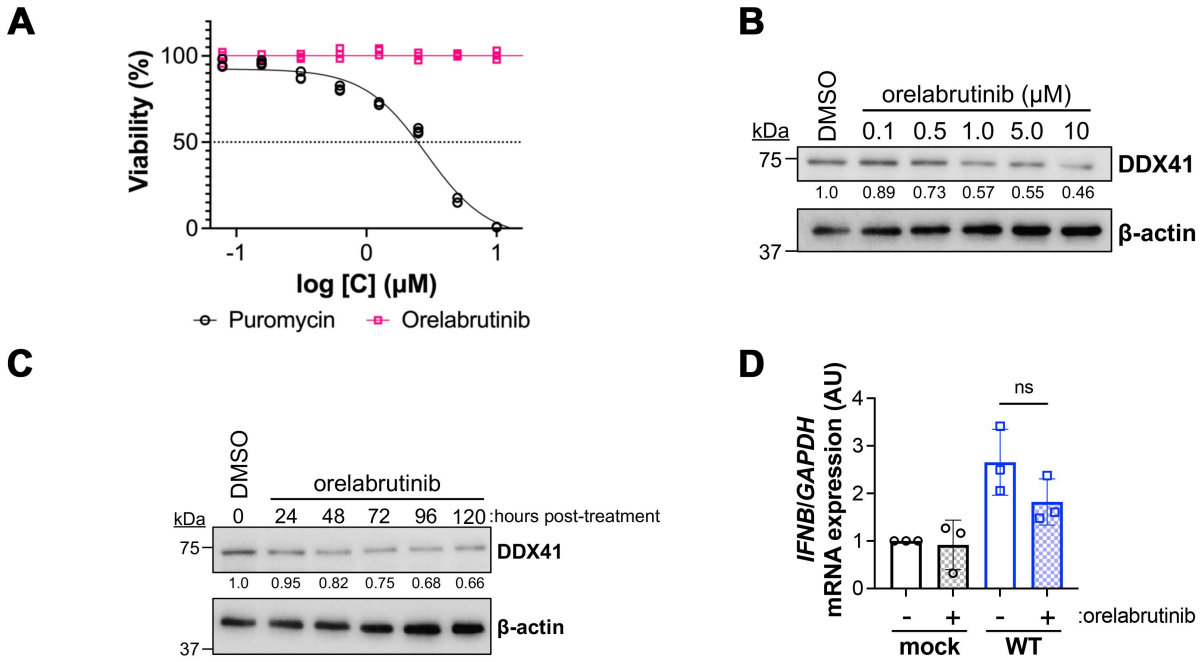

Figure S2. The BTK inhibitor, orelabrutinib, attenuates DDX41 abundance and *IFNB* expression, with no impact on cell viability. (**A**) NuFF-1 fibroblasts were incubated with orelabrutinib (pink; 0.08 μM – 20 μM) for 96 h. Counterpart cultures were treated with puromycin (black; 0.08 μM – 20 μM) as a positive control. Cell viability was assessed by CellTiter-Glo assay. Each concentration within a biological replicate was assessed in triplicate (indicated by datapoints). N = 3; representative assay shown. (**B**) NuFF-1 fibroblasts were treated with either orelabrutinib (0.1 – 10 μM) or DMSO (v/v). After 96 h, cells were harvested, and cell lysates (25 μg) were probed for DDX41 and cellular actin. N = 3; representative blots shown. (**C**) NuFF-1 fibroblasts were treated with 0.5 μM orelabrutinib or DMSO (v/v). Cells were harvested at the indicated times post-treatment and cell lysates (25 μg) were probed for DDX41 and cellular actin. (**B,C**) Abundance of DDX41 relative to β-actin was quantified by densitometry, relative to the DMSO control. N = 3; representative blots shown. (**D**) NuFF-1 fibroblasts were pre-treated with 0.5 μM orelabrutinib or DMSO (v/v) 1 h prior to mock (black) or WT (blue) infection (MOI=0.5 $TCID_{50}$/cell). Cells were harvested 96 hpi, total RNA was isolated, and *IFNB* mRNA expression was quantified by RT-qPCR. Data is plotted as ΔΔCt for *IFNB* relative to *GAPDH* in arbitrary units (AU). Each sample within a biological replicate was analyzed in triplicate (datapoints). Error bars indicate the SD of the mean of three biological replicates. ns, not significant. N = 3; representative assay shown.

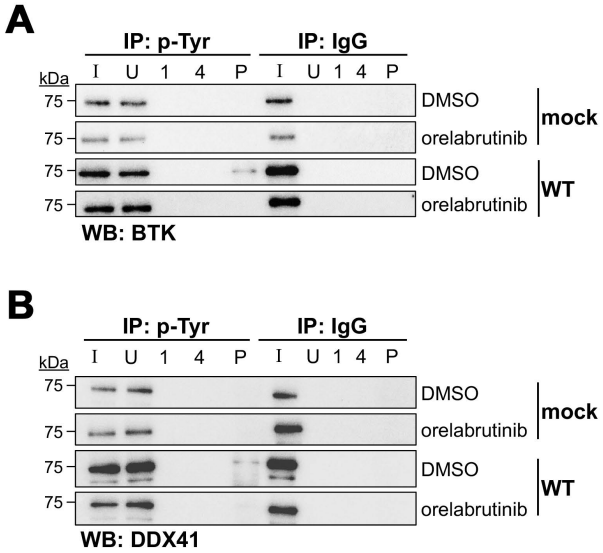

Figure S3. Orelabrutinib inhibits CMV-induced DDX41 and BTK phosphorylation. NuFF-1 fibroblasts were pre-treated with 0.5 μM orelabrutinib or DMSO (v/v) 1 h prior mock or WT infection (MOI = 0.5 $TCID_{50}$/cell) for 96 h. Cells lysates were immunoprecipitated (IP) with antibodies specific for phosphorylated-Tyrosine (p-Tyr) or IgG. Immunoprecipitates were then probed for (**A**) BTK or (**B**) DDX41 by western blot (WB). I, input; U, unbound; 1, wash #1; 4, wash #4; P, IP sample. N = 3; representative blots shown.